Dyes and Pigments 224 (2024) 112045

Contents lists available at ScienceDirect

Dyes and Pigments

journal homepage: www.elsevier.com/locate/dyepig

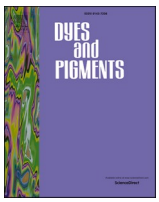

Efficient triisopropylsilylethynyl-substituted benzo[1,2-*b*:4,5-*b*′] dithiophene-based random terpolymers enable non-fullerene organic solar cells with enhanced efficiency

Nam Gyu Yang, Gururaj P. Kini, Hyoung Seok Lee, Ji Youn Kim, Doo Kyung Moon *

Nano and Information Materials (NIMs) Laboratory, Department of Chemical Engineering, Konkuk University, 120, Neungdong-ro, Gwangjin-gu, Seoul, 05029, South Korea

A B S T R A C T

Recent work has highlighted the pivotal role of ternary random polymers in the development of efficient high-performance polymer donors for organic solar cells (OSCs) and most of these D-A copolymer donors are so far constituted of an equal proportion of D and A-units. In this contribution, we report series of PM6-based ternary random terpolymers with unequal D- and A-units, namely, PM-TIPS10, PM-TIPS20 and PM-TIPS20, respectively by adding the 10%, 20% and 30% of simple and low-cost triisopropylsilylethynyl-substituted benzo[1,2-*b*:4,5-*b*′]dithiophene (BDT-TIPS) unit as second donor (D1) unit in polymer backbone based on D1-A-D2-A molecular design. Ascribed from the structural similarity of the two building blocks in the terpolymer backbone, these polymers showed orderly molecular packing, broadened light absorption, and the face-on orientation of the active layer to facilitate charge transport. Additionally, the new polymers displayed much deeper highest occupied molecular orbital (HOMO) energy levels than host PM6 polymer, which helped in enhancing the open circuit voltage (*Voc*) in the PM-TIPS-based OSCs. As a result, when combined with BTP-eC9 acceptor unit, PM-TIPS10 and PM-TIPS20 displayed best efficiency of 16.7 and 16.5% with a small energy loss of 0.484 and 0.473 eV, producing overall superior device parameters compared to PM6-based devices tested parallelly (PCE of 15.7%). This study reveals the correlation between introduction of the BDT-TIPS unit on polymer properties and photovoltaic performance and thus contributes to the design of high-PCE polymer donors by adapting a ternary random copolymerization strategy.

1. Introduction

Organic solar cells (OSCs) have developed rapidly and attracted attention both from academia and industry, because of their useful properties such as solution-processability, mechanical flexibility, light weight, semitransparency and scalability [1–6]. Typically, the active bulk heterojunction (BHJ) layer of OSCs is composed of conjugated polymer donor (p-type) and a polymer or small molecule acceptor (n-type). In the past few decades, with the rapid advancement of organic photoactive materials and device fabrication techniques, power conversion efficiency (PCE) of the OSCs has sharply increased. Particularly, the emergence of small molecule non-fullerene acceptors, e.g. ITIC, Y6 and their modifications [7–10] and wide bandgap conjugated polymer donors [11–14], led to this remarkable improvement of PCEs of OSCs up to 18–19% [14–19].

At present, the PM6 polymer donor comprising of alternate fluorinated thionyl-benzodithiophene (F-BDT) and benzodithiophenedione (BDD) as donor and acceptor unit, respectively is considered as most compatible and reference polymer donor for emerging Y6-based OSCs [20,21]. However, so far, this PM6:Y6-based system has shown PCES of only ≈16%, and PM6 has high synthetic cost because of the multi-step synthesis of the BDTT and the BDD. Therefore, along with the lowering of the synthetic cost of PM6 and improving the PCEs is considered as great significance for OSC commercialization. Several strategies such as (i) grafting functional groups (e.g., F, Cl and ester group) on the backbone to fine-tune the energy levels and crystallinity [5,21–25]; (ii) tailoring the side-chain to improve solubility and morphology [26–31] and (iii) synthesizing ternary polymers based on PM6 have been developed to further boost the PCEs of PM6:Y6 system were already attempted [20,21]. Relative to optimizing the structure of donor polymer by adjusting the chemical structures by molecular reconstruction or modification which involves tedious synthesis, ternary random D-A (where, D is electron-donating unit and A is electron-accepting unit, respectively) copolymerization strategy by introducing third component (D2 or A2 unit) into a molecular design of D-A polymers is evolved as a most reliable and facile method for further fine-tuning the properties of corresponding host polymers [19,32–36]. Recently, several reports have demonstrated that developing terpolymers either adopting D–A1–D–A2 or D1–A–D2–A-type is an effective strategy to tailor the energy levels, absorption, and charge transfer

* Corresponding author.
E-mail address: dkmoon@konkuk.ac.kr (D.K. Moon).

https://doi.org/10.1016/j.dyepig.2024.112045
Received 29 November 2023; Received in revised form 16 February 2024; Accepted 19 February 2024
Available online 20 February 2024
0143-7208/

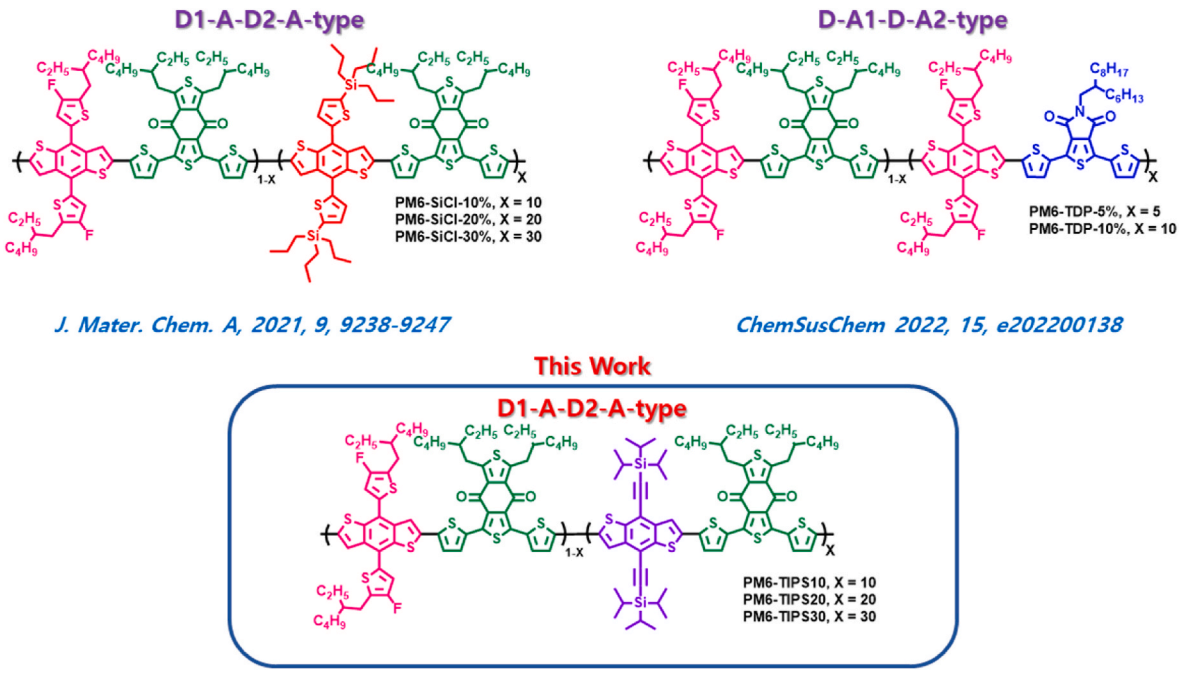

Scheme 1. Chemical structures of the representative D–A1–D–A2 (D1–A–D2–A)-type ternary random terpolymers by combining a third component (D2 or A2 unit) *versus* current study having unequal D- and A-units, which is based on D–A–D–D1molecular design.

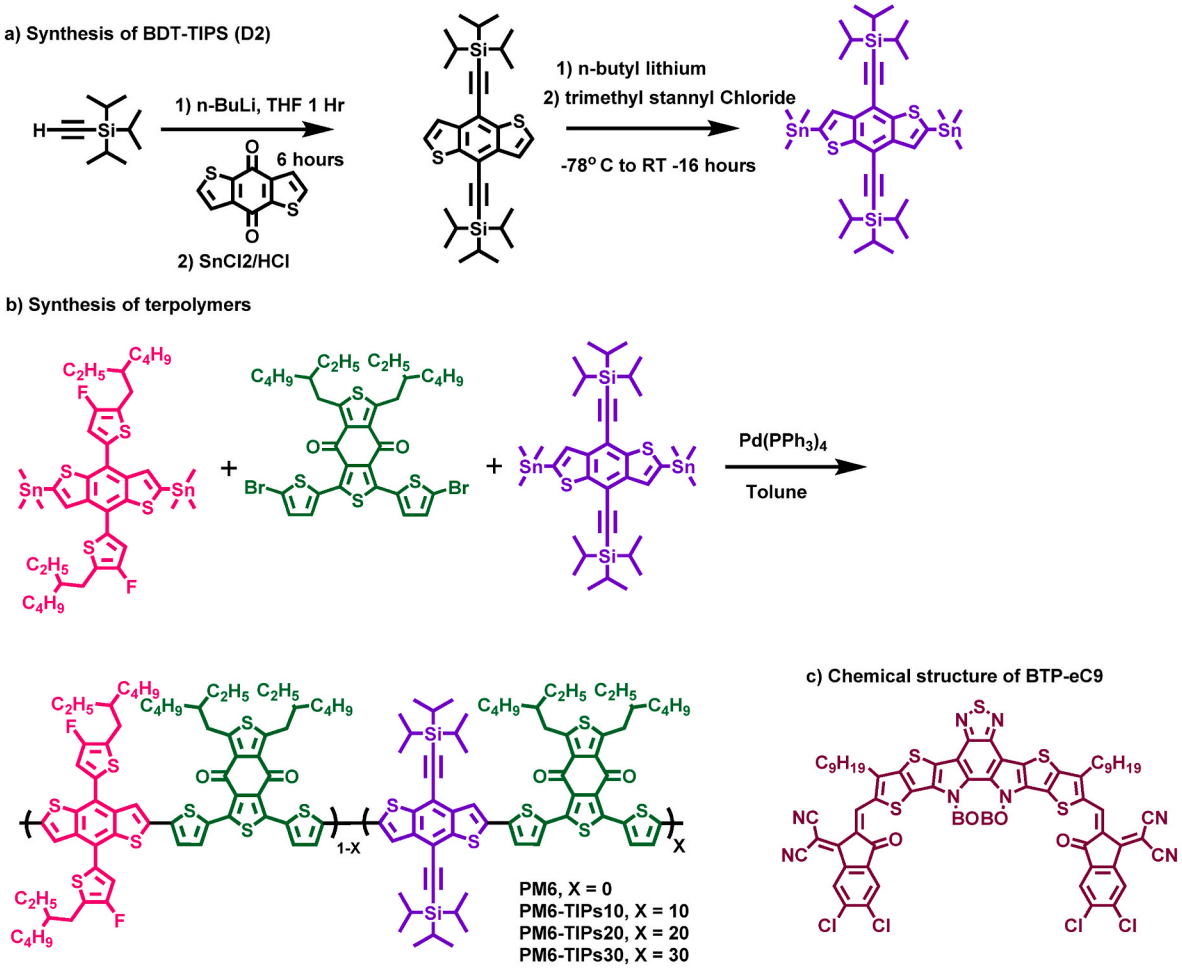

Fig. 1. Synthetic routes of the a) BDT-TIPS, b) terpolymers and c) chemical structure of BTP-eC9.

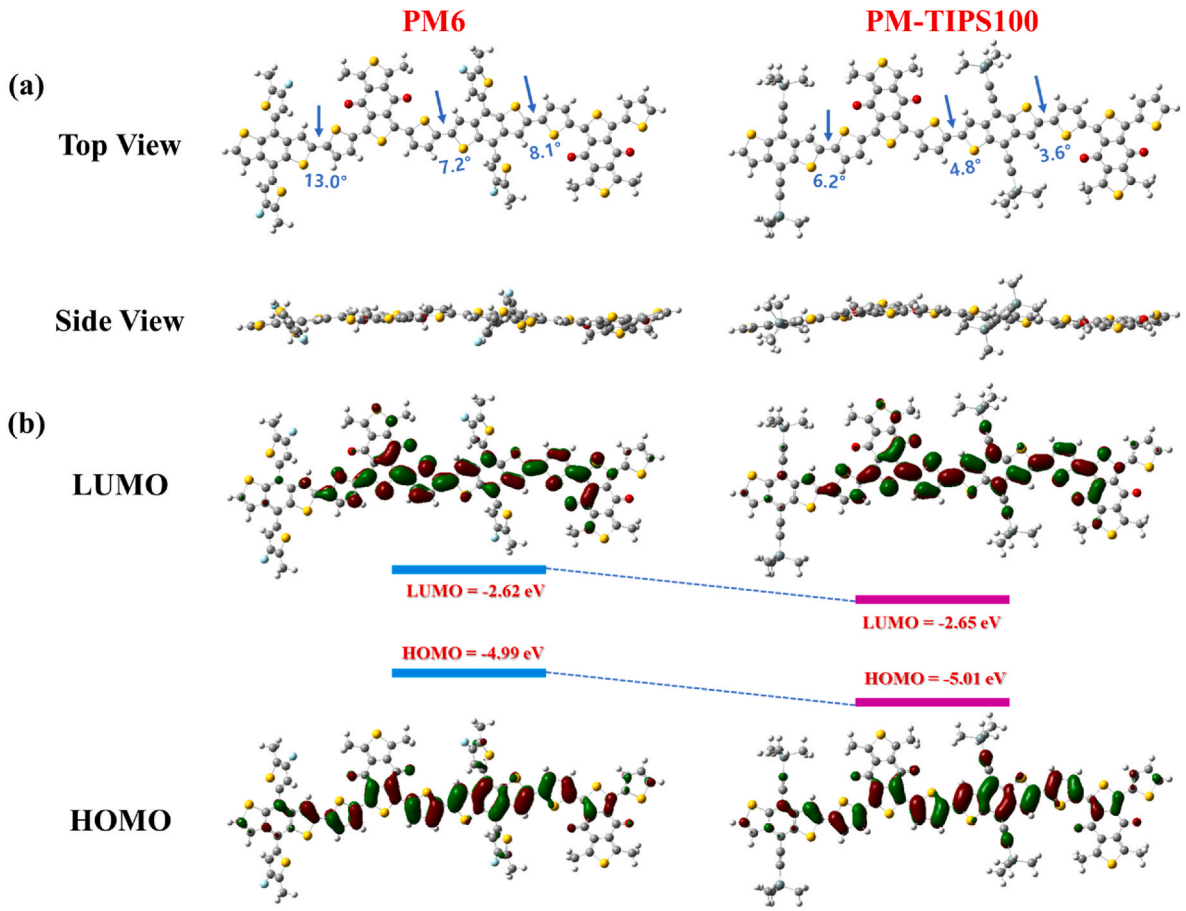

Fig. 2. a) Chemical geometry of the molecular models for PM6 and PM-TIPS. b) molecular energy levels and wave function distributions of the frontier orbits for the polymer models.

properties, without compromising aggregation and desired blend morphology of the binary blend [19,32–37]. For example, Yang and co-workers incorporated Si and Cl functionalized benzodithiophene (BDT-SiCl) as D2 into PM6-backbone, and the corresponding terpolymer exhibited further deepened electronic energy levels and red-shifted absorption. Consequently, the OSC based on terpolymer PM6-SiCl-10% (with 10% BDT-SiCl) as donor and Y6 as acceptor yielded over 16% PCE [38]. In 2020, Wu et al. reported another PM6-based random terpolymers named as PM1 by grafting 20% thiophene-thiazolothiazole (TTZ) as A2-unit. This polymer showed highest PCE of 17.6%, with effectively tailored deep highest occupied molecular orbital (HOMO) energy level, molecular orientation and blend morphology [39]. Very recently, Li and co-workers demonstrated that new polymer PZ-T polymer having deep-lying energy levels as well as favorable packing properties, realized by adding different amounts of 2,5-bis(4-(2-ethylhexyl)thiophen-2-yl) pyrazine unit into the PM6-backbone. Among these PMZ-10:Y6 demonstrate efficient exciton dissociation, higher and balanced electron/hole mobilities, superior aggregation and morphology, and thus realizing high PCE of 18.23% [19].

Herein, we synthesized a series of D1-A-D2-A type PM6-based random terpolymers comprising of two donor units 4,8-bis(5-(2-ethylhexyl)-4-fluorothiophen-2-yl)benzo[1,2-*b*:4,5-*b*′]-dithiophene (BDT-F, D1), and ((2,6-bis(trimethylstannyl)benzo[1,2-b:4,5-b']dithiophene-4,8-diyl)bis(ethyne-2,1-diyl))bis(triisopropylsilane) (BDT-TIPS, D2) and one electron-deficient 1,3-bis(thiophen-2-yl)-5,7-bis(2-ethylhexyl) benzo-[1,2-*c*:4,5-*c*′]dithiophene-4,8-dione (BDD, A) as the acceptor unit (Scheme 1). We selected a triisopropylsilylethynyl (TIPS)-substituted BDT (BDT-TIPS) as the second donor unit in our molecular design because benefits of addition of TIPS group in molecular design such as a) aiding good solubility, high oxidation stability, higher charge transport owing to the effective π-orbital overlap between backbone and silicon atom, and thus yielded remarkable success in realizing excellent PCEs in binary OSCs [27,40–43]. b) BDT-TIPS has same BDT backbone as the parent BDT-2F donor in the PM6-design, hence it can minimize the variation of molecular orderly packing triggered by the random copolymerization and subsequently facilitate favorable morphology and face-on molecular orientation, provided optimal ratio of BDT-TIPS is introduced PM6 matrix. c) σ*(Si)–π*(C) bonding interaction and strong electron-withdrawing carbon-carbon triple bonds in triisopropylsilylethynyl side-chain (see ESP distribution in Fig. S1.) offers further downshifted energy levels, hence can aid in boosting the open-circuit voltage (V_{oc}) in corresponding OSCs [41]. d) BDT-TIPS has low-cost and simple synthesis among the substituted BDT-analogues as shown in Scheme S2. Thus, combining the distinctive advantages of BDT-TIPS and random copolymerization, we report a series of new PM-TIPs based terpolymers, namely, PM-TIPS10, PM-TIPS20 and PM-TIPS30 with varied ratios of BDT-TIPS (D2) units from 10, 20 and 30%, respectively in the PM6-molecular design for efficient OSCs. As expected, it was observed that stepwise increase of molecular percentage of BDT-TIPS caused subtle change in the optical property, energy levels, and molecular packing. By combining with the Y6-based BTP-eC9 acceptor core, corresponding OSCs were fabricated to examine the photovoltaic performance of these terpolymers. Among them, the PM-TIPS10 and PM-TIPS20-based OSC exhibited the best PCE of 16.7 and 16.43% with corresponding V_{OC} of 0.836 and 0.847V, respectively, which is higher than of reference PM6 (15.7% and 0.824V) copolymer tested parallelly. The in-depth study revealed that the improved photoelectric performance of the PM-TIPS10 and PM-TIPS20 is mainly

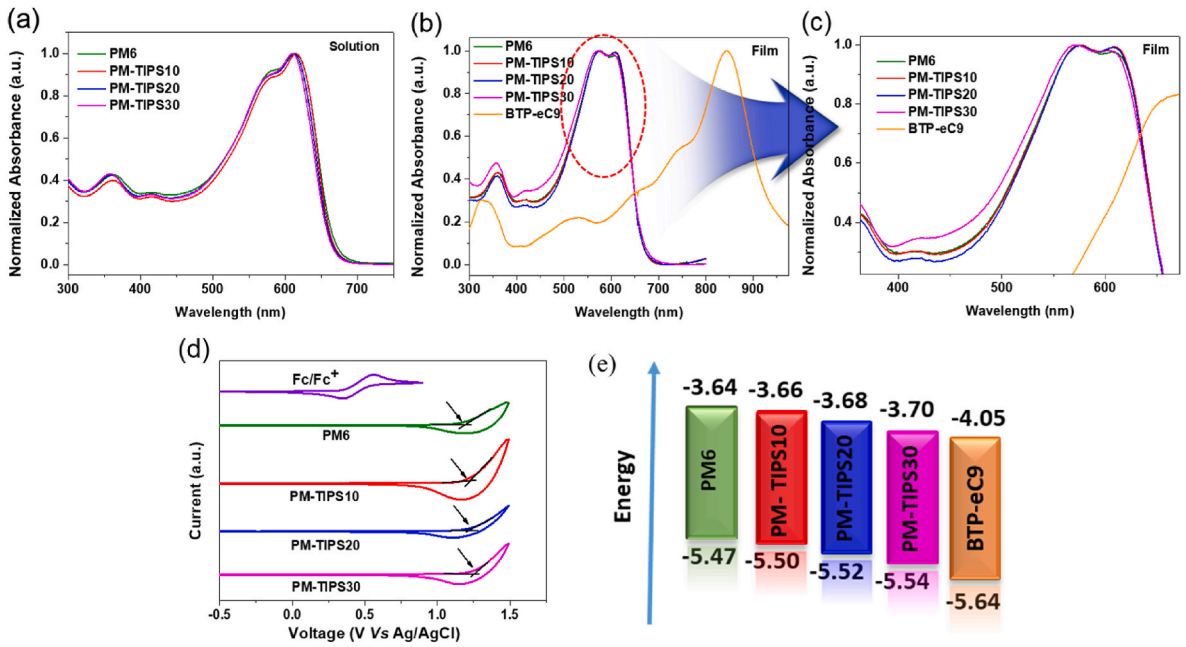

Fig. 3. Absorption spectra of the new polymers in a) CF solutions, b) the thin-film state, c) enlarged section of thin-film state, d) cyclic voltammograms and e) energy level diagram of polymers and BTP-eC9 used in this study.

Table 1
The optical properties and frontier energy levels of related donor polymers.

Polymer	M_n [kDa]/PDI[a]	Optical properties				Electrochemical properties	
		λ_{max} [nm], solution	λ_{max} [nm], thin film	λ_{onset} [nm], thin film	E_g^{opt} [eV][b]	HOMO [eV]^{CV}	LUMO [eV]^{CV}
PM6	33.89/2.21	614	574, 608	677	1.83	−5.47	−3.64
PM-TIPS10	38.64/2.05	615	575, 609	674	1.84	−5.50	−3.66
PM-TIPS20	37.04/2.19	612	572, 604	673	1.84	−5.52	−3.68
PM-TIPS30	36.72/2.28	610	572, 604	675	1.84	−5.54	−3.70

[a] Measured by GPC.
[b] $E_g^{opt} = 1240/\lambda_{onset}$ (neat film), eV.

ascribed from the good energy level alignment, reduced energy loss (E_{loss}), favorable face-on molecular orientation and optimal morphology, which favors higher and balanced charge carrier mobility by minimizing charge recombination. Our findings indicate that BDT-TIPS is a promising building block for designing high-performance and low-cost conjugated materials for OSCs.

2. Results and discussion

The synthetic routes to the monomers, chemical structures of polymers and BTP-eC9-4F were shown in Fig. 1. The molar ratios of D1:D2 for PM6, PM-TIPS10, PM-TIPS20 and PM-TIPS30 are 1:0, 0.9:0.1, 0.8:0.2 and 0.7:0.3, respectively, while the molar ratio of D_{1+2}:A was fixed to be 1:1. The polymerization was carried out via Stille coupling reaction using $Pd(PPh_3)_4$ as the catalyst in toluene solvent. Finally, the crude polymers were precipitated in methanol and then purified by Soxhlet extraction with methanol, acetone, hexane and chloroform, respectively. The detailed synthetic procedures of monomers and polymers along with their detailed characterization, were provided in supporting information. All optimized polymers exhibited good solubility in organic solvents, such as chloroform (CF) or chlorobenzene (CB). By using the gel permeation chromatography (GPC), the number-average molecular weights (*M*n) of PM6, PM-TIPS10, PM-TIPS20 and PM-TIPS30 terpolymers were estimated to be around 33–38 kDa, respectively with corresponding polydispersity (PDI) values of 2.05–2.28. Further, thermal stabilities of the polymers were determined using thermogravimetric analysis (TGA). The thermal decomposition temperatures of PM6, PM-TIPS10, PM-TIPS20 and PM-TIPS30 were found to be 373, 385, 362 and 366 °C, respectively, with a 5% weight loss (Fig. S2).

As shown in Fig. 2, Density functional theory (DFT) calculations at B3LYP/6-31G (d, p) basis set was carried out to examine the impact of insertion of BDT-TIPS unit on the molecular geometry and electronic structures terpolymer backbone. Meanwhile, to get acceptable computing load, these calculations were performed based on the dimeric structures of the polymers and the alkyl chains were replaced with the methyl chains. As shown in Fig. 2a, PM-TIPS100 has a smaller dihedral angle of 6.2°, 4.8° and 3.6° between BDT-TIPS and BDD units, whereas PM6 showed angle of 13.0°, 7.2° and 8.1° for BDT-F and BDD, suggesting insertion of BDT-TIPS enhances coplanarity of the polymer. Planar polymer have advantage in facilitating the superior intermolecular packing and can facilitate better charge transport and FF in the devices [35]. Further, frontier molecular orbitals (FMO) energy levels profile both polymer structures showed identical electron density distribution profiles with completely delocalized HOMO and LUMO energy levels on the entire polymer backbone (Fig. 2b). Also, originating from the strong electronegativity of TIPS side chain [40,44,45] and the calculated HOMO/LUMO energy levels of PM-TIPS100 were found to be lower −5.01/-2.65 eV than PM6 (−4.99/-2.62 eV), which suggesting the introduction of BDT-TIPS could aid in lowering the FMO energy levels in corresponding terpolymers and in turn will contribute to achieve higher V_{OC} in the terpolymers related OSCs. These observations aggreging well with the cyclic voltammetry measurements (discussed subsequently).

The optical properties of the new polymer were estimated using the

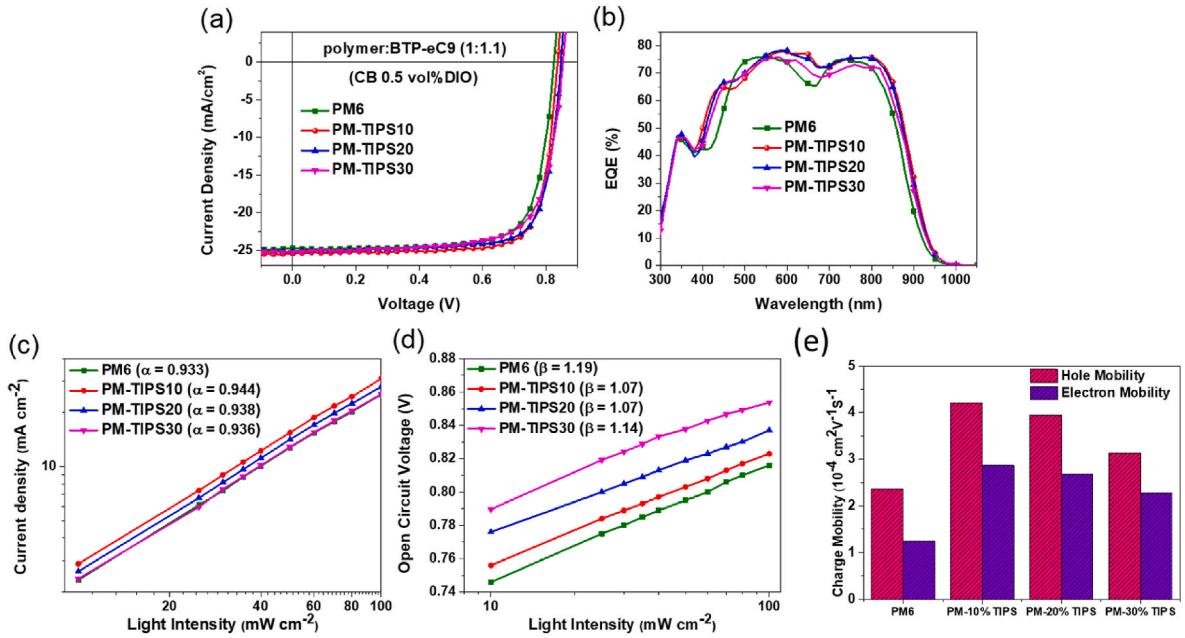

Fig. 4. a) $J-V$ curves and b) EQE profiles of the optimized polymer:BTP-eC9 OSCs under illumination of AM1.5G, 100 mW $cm^{2,}$ respectively. **c**) J_{SC} and d) V_{OC} as a function of the incident light intensity, respectively. e) The charge carrier mobility of the blend films based on polymer donors:BTP-eC9.

Table 2
Photovoltaic parameters of the different polymer:BTP-eC9 OSCs blend films (1:1.1) (w/w) processed using CB + 0.5 vol% DIO and thermal annealing treatment at 100 °C for 10 min under the illumination of AM 1.5G, 100 $mWcm^{-2}$.

Active layer	V_{OC} [V]	J_{SC} [mA/cm^2]	J_{SC}^{EQE} [mA/cm^2]	*FF* [%]	PCE [%]	E_g^{onset} (eV)[a]	E_{loss} [eV][b]	R_{sh} [$k\Omega cm^2$]	R_s [Ωcm^2]
PM6:BTP-eC9	0.824 (0.822 ± 0.015)	25.03 (25.0 ± 0.03)	23.84	76.18 (75 ± 1.18)	15.70 (15.63)	1.33	0.506	1.11	3.19
PM-TIPS10:BTP-eC9	0.836 (0.830 ± 0.006)	25.43 (25.0 ± 0.6)	23.93	78.48 (78 ± 0.48)	16.70 (16.61)	1.32	0.484	1.46	2.14
PM-TIPS20:BTP-eC9	0.847 (0.84 ± 0.007)	25.12 (25.0 ± 0.24)	23.87	77.19 (77 ± 0.22)	16.43 (16.41)	1.32	0.473	1.30	2.29
PM-TIPS30:BTP-eC9	0.853 (0.85 ± 0.003)	24.84 (24.0 ± 0.84)	23.72	74.76 (74 ± 0.76)	15.85 (15.78)	1.33	0.477	0.72	4.03

Device architecture: ITO/PEDOT:PSS/active layer/PDINN/Ag (conventional).
[a]The average values and standard deviations were derived from 8 to 10 independent devices.
[a] Eg^{onset} is the optical gap of the main light absorber, which is calculated from the EQE spectrum.
[b] $E_{loss} = Eg^{onset} - qV_{OC}$, where q is the elementary charge [49].

Table 3
Hole and electron mobility of the polymer:BTP-eC9 blends derived from the SCLC method.

Blend system	μ_h ($cm^2\ V^{-1}\ s^{-1}$)	μ_e ($cm^2\ V^{-1}\ s^{-1}$)	μ_h/μ_e
PM6:BTP-eC9	2.37×10^{-4}	1.25×10^{-4}	1.89
PM-TIPS10:BTP-eC9	4.21×10^{-4}	2.87×10^{-4}	1.47
PM-TIPS20:BTP-eC9	3.95×10^{-4}	2.68×10^{-4}	1.47
PM-TIPS30:BTP-eC9	3.14×10^{-4}	2.28×10^{-4}	1.38

μ_h = hole mobility and μ_e = electron mobility.

UV–vis absorption spectroscopy. The corresponding absorption profiles of the polymers in chloroform solution and thin-film states were shown in Fig. 3a–c and corresponding photophysical parameters are summarized in Table 1. All three polymers showed nearly similar absorption profiles like PM6 with broad absorption band ranging from 400 to 700 nm, with corresponding absorption maximum located ~615 nm in solution state and at ~610 nm in the thin film state. Meanwhile, attributed to the stronger intermolecular π–π stacking, the absorption profile of polymers in the film states becomes much broader, and red-shifted than solution state. Interestingly, compared to PM6, the absorption profiles of the PM-TIPS10 and PM-TIPS20 slightly red-shifted with accompanied by a gradually increased 0-0 transition peak at about 611 nm, suggesting that the terpolymers have a more ordered polymer chain stacking than parent PM6 (Fig. 3c). In contrast, PM-TIPS30 gradually showed blue-shifted absorption (with pronounced 0–1 transition at 573 nm and decreased 0-0 transitions at 609 nm), which suggesting increased amounts of BDT-TIPS causing weaker ICT and packing. From the absorption edges of the polymers in the film state, the corresponding optical band gaps (E_g^{opt}) estimated to be 1.83, 1.84, 1.84 and 1.83 eV for PM6, PM-TIPS10, PM-TIPS20 and PM-TIPS30, respectively (Table 1). Moreover, as shown in Fig. 3b, all these polymers have good complementary absorption with BTP-eC9 acceptor and thus favoring the improving photocurrent in relative OSCs by covering the broad spectral ranging from 300 to 950 nm.

The effect of BDT-TIPS proportion of on the frontier energy levels of the copolymers were evaluated using Cyclic voltammetry (CV). The cyclic voltammograms of the polymers and energy level alignment of polymers and BTP-eC9 used in this study are shown in Fig. 3d and e. The E_{HOMO} of the PM6, PM-TIPS10, PM-TIPS20 and PM-TIPS20 estimated to be −5.47, −5.50 and −5.52 and −5.54 eV, respectively calculated using the equation: $E_{HOMO} = -e\ (E_{ox/red} + 4.8 - E_{Fc/Fc}^{+})$ (where $E_{ox/red}$ is the

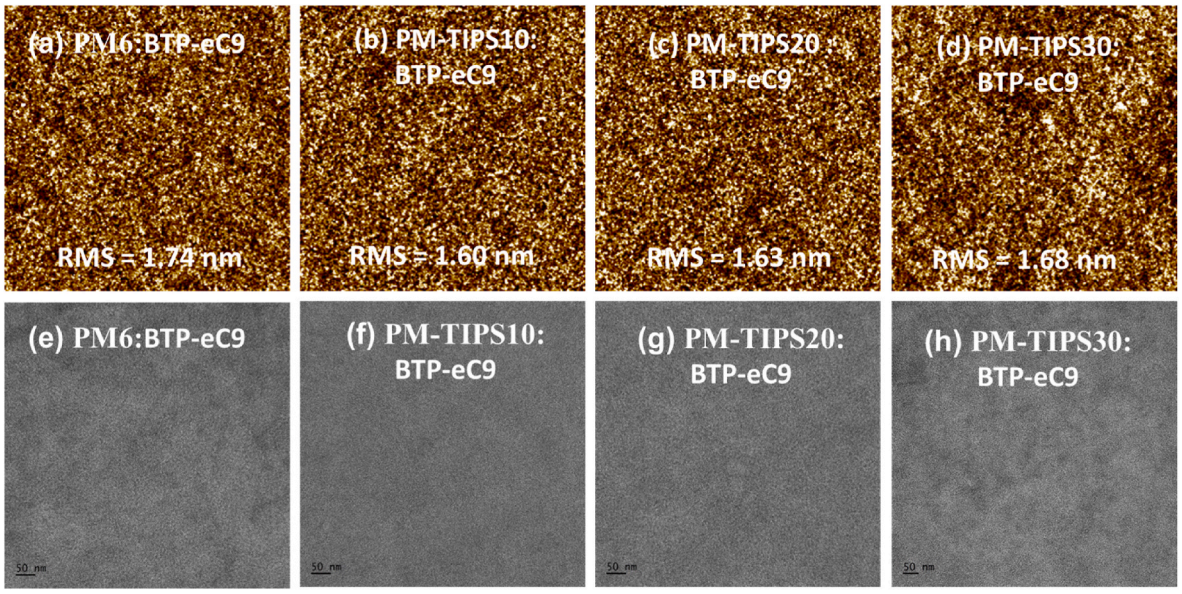

Fig. 5. AFM and TEM images of optimal blend films based on (a, e) PM6: BTP-eC9, (b, f) PM-TIPS10:BTP-eC9, (c, g) PM-TIPS20:BTP-eC9 and (d, h) PM-TIPS30: BTP-eC9.

onset oxidation potentials measured against the Ag/AgCl as reference electrode and redox potential of ferrocene $E^{+}_{Fc/Fc}$ is used as an internal standard, respectively). Meanwhile, LUMOs are calculated to be −3.64, −3.66, −3.68 and −3.70 eV, respectively for PM6, PM-TIPS10, PM-TIPS20 and PM-TIPS30, respectively, which is estimated from the equation $E_{LUMO} = E_g^{opt} - E_{HOMO.}$ As expected, introduction of BDT-TIPS content gradually decreased both HOMO and LUMO energy levels, which is originated from the strong electronegativity of TIPS side chain [40,44,45]. Thus, the deeper HOMOs of the newly synthesized polymers not only aid in further stabilizing the polymers, but are also helpful in improving the V_{OC} and lowering the energy losses in the OSCs.

We evaluated the photovoltaic performance of this series of terpolymers by fabricating OSCs with a conventional device structure of ITO/poly(3,4- ethylenedioxythiophene):poly(styrenesulfonate) (PEDOT:PSS)/Polymer:BTP-eC9/PDINN/Ag. Initially, D/A ratio, spinning speed, different solvent/additive and different acceptor were screened to realize the best optimized conditions (Figs. S3–S7 and Tables S1–S6). The current-density–voltage (*J–V*) curves of the optimized devices are shown in Fig. 4a and with the corresponding detailed photovoltaic parameters were summarized in Table 2. As anticipated, relative to the control PM6-based devices which has demonstrated the V_{oc} of 0.824V, V_{oc} of terpolymers were systematically enhanced 0.836, 0.847 and 0.853 V for PM-TIPS10, PM-TIPS20 and PM-TIPS30, respectively. These trends agreed with the tendency of their lower HOMO energy levels of the newly synthesized terpolymers, which originated from the increase in the BDT-TIPS content from 10% to 30%. Meanwhile, among the terpolymers, the optimal devices based on PM-TIPS10:BTP-eC9 exhibit an highest PCE of 16.7%, with corresponding photovoltaic parameters V_{oc} of 0.836 V, short circuit current density (J_{sc}) of 25.43 mA cm^{-2} and fill factor FF of 78.48%, with respect to the control devices based on PM6: BTP-eC9 show relatively lower PCE of 15.87% (V_{oc} of 0.824 V, J_{sc} of 25.03 mA cm^{-2} and FF of 76.18%). Notably, in addition to the enhancement of V_{oc}, addition of 10% BDT-TIPS also favored the improvement of J_{sc} and FF, suggesting the positive effect on the morphology and the crystallinity of the blend film. Meanwhile, further increasing the BDT-TIPS proportion from 20% in PM-TIPS20 and 30% in the case of PM-TIPS30 results in a slight drop in the device efficiency, corresponding devices showed decent PCEs of 16.43% (V_{oc} of 0.847 V, J_{sc} of 25.12 mA cm^{-2}, FF of 77.19%) and 15.84% (V_{oc} of 0.853 V, J_{sc} of 24.84 mA cm^{-2}, FF of 74.76%), respectively. Though PM-TIPS20 and PM-TIPS30 devices showed higher V_{oc}, these results clearly showed the introduction of BDT-TIPS unit causing a substantial decrease in the J_{sc} and FF. Series resistance (R_s) and shunt resistance (R_{sh}) were calculated from *J-V* curve under 1.0 sun illumination, and dark *J-V* curves were also plotted to further analyze this phenomenon. It is well known that R_s and R_{sh} affects J_{SC} and FF of the OSC devices. Calculated R_s were 3.19, 2.14, 2.29 and 4.03 Ωcm^2 for PM6, PM-TIPS10, PM-TIPS20 and PM-TIPS30 based devices. And R_{sh} were calculated to be 1.11, 1.46, 1.30 and 0.72 kΩcm^2 for PM6, PM-TIPS10, PM-TIPS20 and PM-TIPS30 based devices. PM-TIPS10 based device showed the lowest R_s and the highest R_{sh}, which matches well with the highest J_{SC} and FF of PM-TIPS10 based device. Furthermore, as can be seen from dark *J-V* curve in Fig. S10, the leakage current of PM-TIPS10 based device seemed to be much lower than other devices, which also agrees well with the photovoltaic parameters under 1.0 sun illumination.

Using the equation $E_{loss} = Eg - eV_{OC}$ (E_g^{onset} was obtained from the EQE spectrum), the energy losses (E_{loss}) of the optimal devices were estimated (Table 2) [46]. Remarkably, the PM6, PM-TIPS10, PM-TIPS20 and PM-TIPS30-based devices showed lower E_{loss} values of 0.484, 0.473 and 0.477 eV, respectively (*versus* PM6, which is 0.506), which are among rarest few examples having E_{loss} <0.5 eV reported to date to the best of our knowledge [47–49].

The external quantum efficiency (EQE) curves of the optimized devices are shown in Fig. 4b were recorded to systematically understand the reason behind the variation in *Jsc* values. The EQE spectrum of all polymers were comparable with their absorption profiles and all the terpolymers have a broad and high photo response 300–950 nm wavelength region. The J_{SC} values estimated from the EQE profiles were well-matched with values from the *J-V* measurements. Among the terpolymers, the device based on PM-TIPS10:BTP-eC9 and PM-TIPS20:BTP-eC9 exhibits higher responses almost entire wavelength region of 550–950 nm with EQE values over 75% and peak value reaching around 85% at ca. 600 nm, thereby justifying their higher *Jsc* values in their optimal devices. In contrast, PM6:BTP-eC9 and PM-TIPS30:BTP-eC9 displayed comparatively slightly lower EQE values.

The charge recombination behavior of OSCs were probed qualitatively by checking the effect of J_{SC} and V_{OC} under various illumination light intensity, which is described by the equation of power $J_{SC} \propto I^{\alpha}$, where I and α are incident light intensities and exponential constant, respectively. Generally, when the α value is close to 1, it indicates bimolecular recombination is weaker or minimal [19,28,50]. In the current series, α value is 0.933, 0.944, 0.938 and 0.936 for PM6: BTP-eC9, PM-TIPS10:BTP-eC9, PM-TIPS20:BTP-eC9 and PM-TIPS30:

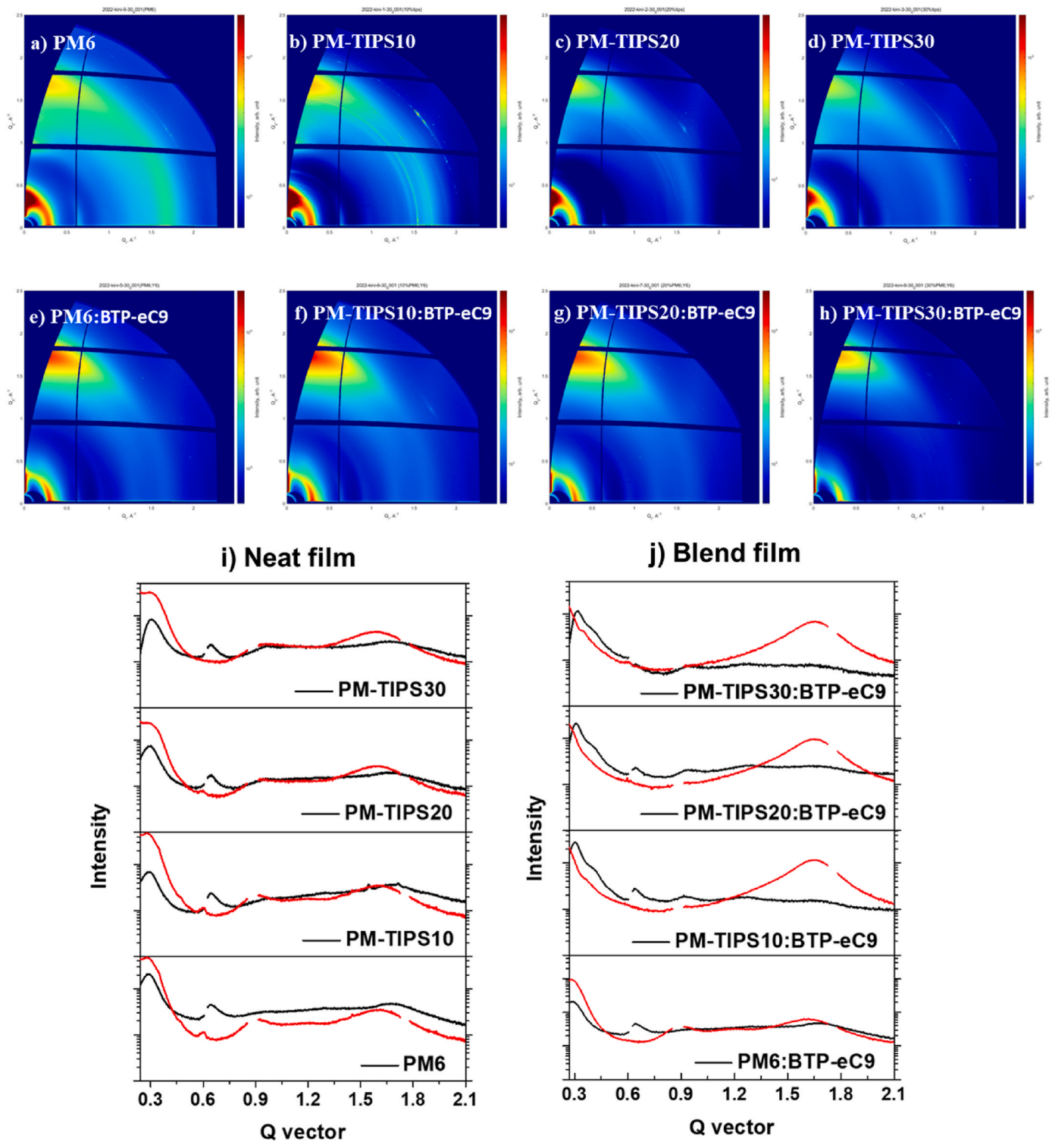

Fig. 6. (a–h) 2D GIWAXS patterns and (i–j) 1D GIWAXS line curves with corresponding in-plane (IP) and out-of-plane (OOP) profiles of pristine polymer donors and blend films with BTP-eC9.

BTP-eC9, respectively (Fig. 4c). Notably, both PM-TIPS10:BTP-eC9, PM-TIPS10:BTP-eC9 have relatively lower α values in the series, thereby yielding higher *J*sc and FF values by suppressed bimolecular recombination in the OSCs and which agrees well with device results. Besides, the formula of $V_{OC} \propto \beta\, k_B T/q\, \ln(I)$ (Fig. 4d), where k, T, and q represent Boltzmann constant, Kelvin temperature, and elementary charge, respectively is used to further investigate mechanism of charge recombination. Generally, slope of kT/q implies the single-molecule recombination are effectively suppressed, whereas slope of 2kT/q suggests that single-molecule recombination dominates in OSCs [19,50]. Thus, in this study the slopes observed were 1.19, 1.07, 1.07 and 1.13, respectively for PM6:BTP-eC9, PM-TIPS10:BTP-eC9, PM-TIPS20:BTP-eC9 and PM-TIPS30:BTP-eC9. This result establishes that the trap-assisted recombination is also effectively suppressed by insertion of BDT-TIPS units in PM6. Collectively, 10–20% loading of BDT-TIPS units aided in enhanced exciton dissociation and charge collection by

Table 4
2D-GIWAXS packing parameters of pristine terpolymers and corresponding blend films with BTP-eC9.

Film	IP[a]		OOP[b]	
	d-(100) [Å]/ (q-(100) [$Å^{-1}$])	d-(010) [Å]/ (q-(010) [$Å^{-1}$])	d-(100) [Å]/ (q-(100) [$Å^{-1}$])	d-(010) [Å]/ (q-(010) [$Å^{-1}$])
PM6	22.04 (0.285)		19.26 (0.326)	3.76 (1.67)
PM-TIPS10	21.22 (0.296)		19.26 (0.326)	3.74 (1.68)
PM-TIPS20	21.73 (0.289)		19.38 (0.324)	3.74 (1.68)
PM-TIPS30	21.73 (0.289)		19.38 (0.324)	3.76 (1.67)
PM6:BTP-eC9	21.51 (0.292)			3.73 (1.68)
PM-TIPS10:BTP-eC9	20.66 (0.304)			3.65 (1.72)
PM-TIPS20:BTP-eC9	20.80 (0.302)			3.65 (1.72)
PM-TIPS30:BTP-eC9	20.94 (0.300)			3.71 (1.69)

[a] Calculation from [a]*xy*-axis and.
[b] z-axis, respectively.

suppressing trap-assisted recombination of devices and consequently aided in boosting the *J*sc and FF in corresponding OSCs.

The charge transport characteristics were further verified by measuring the hole and electron mobilities (μ_h and μ_e) optimal blend films were investigated by the space-charge-limited current (SCLC) method using the device structure of ITO/ZnO/active-layer/PDINN/Ag and ITO/PEDOT:PSS/active layer/MoO_3/Ag devices, respectively. The $J_{1/2}-V$ curves of the corresponding devices are depicted in Fig. S8, and calculated values are summarized in Fig. 4e and Table 3. Notably, compared with PM6: BTP-eC9 blend film ($\mu_h/\mu_e = 2.37 \times 10^{-4}/1.25 \times 10^{-4}$ cm^2 V^{-1} s^{-1}), all the new PM-TIPS-based polymer blends showed higher μ_h and μ_e including the better μ_h/μ_e ratio in the order PM-TIPS10: BTP-eC9 ($4.21 \times 10^{-4}/2.87 \times 10^{-4}$ cm^2 V^{-1} s^{-1}) ≈ PM-TIPS20:BTP-eC9 ($3.95 \times 10^{-4}/2.68 \times 10^{-4}$ cm^2 V^{-1} s^{-1}) > PM-TIPS30:BTP-eC9 ($3.14 \times 10^{-4}/2.28 \times 10^{-4}$ cm^2 V^{-1} s^{-1}). Thus, higher, and balanced charge mobilities are greatly contributing to enhancing FF, *J*sc and overall PCEs by improving effective charge dissociation by minimizing charge recombination [51–53]. Thus, originating from the efficient exciton dissociation and suppressed carrier recombination PM-TIPS10:BTP-eC9 devices realized highest J_{sc} of 25.43 mA cm^{-2} and FF of 78.48% among the terpolymers.

To determine causes for the improved photovoltaic performances of the terpolymers with the addition of appropriate percentage of the BDT-TIPS monomer, atomic force microscopy (AFM) and transmission electron microscopy (TEM) were employed to explore the surface and bulk morphology of these optimal blend films. As shown in the AFM images Fig. 5b–c, PM-TIPS10:BTP-eC9 and PM-TIPS20:BTP-eC9 blend films have uniform and relatively smooth surface morphology with corresponding root-mean-square (RMS) roughness of 1.60 and 1.63 nm, respectively. These nanoscale fibrillar textures with good intermixing of the blend components will certainly contribute to efficient exciton dissociation and charge transport. In contrast, PM6:BTP-eC9-based devices displayed obvious aggregation tendency leading to the relatively higher phase-segregated morphology, which was supported by increased RMS roughness of 1.74 nm (Fig. 5a). Meanwhile, by introducing the 30% of BDT-TIPS, the PM-TIPS10:BTP-eC9 film exhibits have inhomogeneous morphology with formation of tiny clusters of distinct blend components thereby leading to higher RMS roughness of 1.68 nm (Fig. 5d). Such a type of phase segregated morphology will have negative impact not only on the exciton migration via lowering exciton diffusion length, but they also promote charge recombination by acting as a trap sites [54,55]. These observations were in good agreement with TEM images as shown in Fig. 5e–h. The PM-TIPS10:BTP-eC9 and PM-TIPS20:BTP-eC9-based blend films produced more uniform continuous nanofibrillar structures with small length scaled phase separation around 45 nm, which is desirable to balance exciton splitting and carrier transport by forming charge transport pathways [56]. In contrast, both PM6:BTP-eC9 and PM-TIPS20:BTP-eC9-based blend films showed distinct bright and dark domains, suggesting increased phase separation and reason behind the lower FF, *J*sc and PCEs.

To further study the relationship between the molecular ordering, crystallinity and the photovoltaic performance of these D–A–D–D1 copolymers, we performed grazing incidence wide-angle X-ray scattering (GIWAXS) measurements on the pristine copolymer films and their blend films (Fig. 6 and Table 4). As shown in GIWAX images Fig. 6a–d and i, all pristine polymers exhibit a well-defined molecular crystallinity and similar lamellar distances between 19.26 and 19.38 Å, calculated from their respective (100) diffractions in the q_{xy} direction, which is originated from the interpenetration of the side chains. Besides, the (010) peaks increased gradually in the q_z direction from PM-TIPS10 to PM-TIPS20, then to PM-TIPS30, compared with the neat PM6 film. These results indicate an increase of face-on packing tendency that would be favorable for vertical charge transfer in the OSCs [56–59]. The (010) peaks for these four copolymers were located at q_z = 1.67, 1.68, 1.68, and 1.67 $Å^{-1}$, for PM6, PM-TIPS10, PM-TIPS20 and PM-TIPS30, respectively, corresponding to their π–π stacking distances of 3.76, 3.74, 3.74, and 3.76 Å. These results indicated that a stronger π–π stacking and higher coplanarity could be induced by addition of BDT-TIPS, which agrees well with the DFT calculation results. From the GIWAXS patterns of the blended films (Fig. 6e–h and j), the four blended films show a stronger q_{xy} lamellar stacking peak at q = ~0.30 Å, with reduced lamellar distances than pristine film state, which emphasizes blend film processes higher molecular order. Similar trends were also seen in q_z direction, where clear 010 π–π stacking diffraction peak at q = 1.68 $Å^{-1}$ (d_{010} = 3.73 Å), q = 1.72 $Å^{-1}$ (d_{010} = 3.65 Å), q = 1.72 $Å^{-1}$ (d_{010} = 3.65 Å) and q = 1.69 $Å^{-1}$ (d_{010} = 3.71 Å) for the PM6:BTP-eC9, PM-TIPS10:BTP-eC9, PM-TIPS20:BTP-eC9 and PM-TIPS30:BTP-eC9, respectively. Clearly, PM-TIPS10:BTP-eC9 and PM-TIPS20:BTP-eC9 blends having higher crystallinity and preferential face-on molecular orientation among these terpolymers, which in turn contributes to charge carrier transport, consistent with the higher *J*sc, mobility seen in corresponding OSCs.

3. Conclusion

In summary, we have synthesized three new D1-A-D2-A type copolymers (PM-TIPS10, PM-TIPS20 and PM-TIPS30) based on random copolymerization by introducing a simple and low-cost electron-donating triisopropylsilylethynyl-substituted BDT (BDT-TIPS) as the second donor into the popular PM6 copolymer design. Notably, we found that the increased proportion of BDT-TIPS caused the down-shifted the HOMO energy levels of the terpolymers than PM6. Additionally, they also possessed a higher degree of co-planarity, self-assembly and a high crystallinity originated from their similar structures of donor units. Consequently, the terpolymer-based active layers demonstrate suitable energy level alignment with BTP-eC9 acceptor, preferential face-on molecular orientation, higher charge carrier mobility, and desirable morphology. Consequently, the optimal device based on PM-TIPS10:BTP-eC9 accomplished the highest PCE of 16.7% with corresponding photovoltaic parameters V_{oc} of 0.836 V, J_{sc} of 25.43 mA cm^{-2} and FF of 78.48%. This work helps us to understand the synergistic effect of introduction of second donor units into the molecular design of terpolymers on the backbone.

CRediT authorship contribution statement

Nam Gyu Yang: Writing – review & editing, Writing – original draft, Formal analysis, Data curation. **Gururaj P. Kini:** Writing – original draft, Formal analysis, Data curation, Conceptualization. **Hyoung Seok Lee:** Formal analysis, Data curation. **Ji Youn Kim:** Data curation. **Doo Kyung Moon:** Writing – review & editing, Supervision, Project

administration, Funding acquisition, Conceptualization.

Declaration of competing interest

The authors declare that they have no known competing financial interests or personal relationships that could have appeared to influence the work reported in this paper.

Data availability

Data will be made available on request.

Acknowledgements

N.G.Y. and G.P.K. contributed equally to this work. This work was supported by Human Resources Development Program of the Korea Institute of Energy Technology Evaluation and Planning (KETEP) grant funded by the Ministry of Trade, Industry and Energy, Republic of Korea (No. RS-2023-00237035), the Commercializations Promotion Agency for R&D Outcomes (COMPA) grant funded by the Korea government (MSIT) (No. RS-2023-00304788).

Appendix A. Supplementary data

Supplementary data to this article can be found online at https://doi.org/10.1016/j.dyepig.2024.112045.

References

[1] Heeger AJ. 25th anniversary article: bulk heterojunction solar cells: understanding the mechanism of operation. Adv Mater 2014;26:10–28. https://doi.org/10.1002/adma.201304373.
[2] Lu L, Zheng T, Wu Q, Schneider AM, Zhao D, Yu L. Recent advances in bulk heterojunction polymer solar cells. Chem Rev 2015;115:12666–731. https://doi.org/10.1021/acs.chemrev.5b00098.
[3] Lin Y, Jin Y, Dong S, Zheng W, Yang J, Liu A, et al. Printed nonfullerene organic solar cells with the highest efficiency of 9.5. Adv Energy Mater 2018;8:1–8. https://doi.org/10.1002/aenm.201701942.
[4] Yan T, Song W, Huang J, Peng R, Huang L, Ge Z. 16.67% rigid and 14.06% flexible organic solar cells enabled by ternary heterojunction strategy. Adv Mater 2019;31:1–8. https://doi.org/10.1002/adma.201902210.
[5] Kini GP, Jeon SJ, Moon DK. Latest progress on photoabsorbent materials for multifunctional semitransparent organic solar cells. Adv Funct Mater 2021;31:1–32. https://doi.org/10.1002/adfm.202007931.
[6] Du X, Heumueller T, Gruber W, Classen A, Unruh T, Li N, et al. Efficient polymer solar cells based on non-fullerene acceptors with potential device lifetime approaching 10 years. Joule 2019;3:215–26. https://doi.org/10.1016/j.joule.2018.09.001.
[7] Dey S. Recent progress in molecular design of fused ring electron acceptors for organic solar cells. Small 2019;15:1–38. https://doi.org/10.1002/smll.201900134.
[8] Li C, Fu H, Xia T, Sun Y. Asymmetric nonfullerene small molecule acceptors for organic solar cells. Adv Energy Mater 2019;9:1–16. https://doi.org/10.1002/aenm.201900999.
[9] Wang H, Cao J, Yu J, Zhang Z, Geng R, Yang L, et al. Molecular engineering of central fused-ring cores of non-fullerene acceptors for high-efficiency organic solar cells. J Mater Chem A 2019;7:4313–33. https://doi.org/10.1039/c8ta12465e.
[10] Li S, Li CZ, Shi M, Chen H. New phase for organic solar cell research: emergence of Y-series electron acceptors and their perspectives. ACS Energy Lett 2020;5:1554–67. https://doi.org/10.1021/acsenergylett.0c00537.
[11] Fan Q, Su W, Wang Y, Guo B, Jiang Y, Guo X, et al. Synergistic effect of fluorination on both donor and acceptor materials for high performance non-fullerene polymer solar cells with 13.5% efficiency. Sci China Chem 2018;61:531–7. https://doi.org/10.1007/s11426-017-9199-1.
[12] Cao J, Yi L, Zhang L, Zou Y, Ding L. Wide-bandgap polymer donors for non-fullerene organic solar cells. J Mater Chem A 2022;11:17–30. https://doi.org/10.1039/d2ta07463j.
[13] He K, Kumar P, Yuan Y, Li Y. Wide bandgap polymer donors for high efficiency non-fullerene acceptor based organic solar cells. Mater Adv 2021;2:115–45. https://doi.org/10.1039/d0ma00790k.
[14] Pang B, Liao C, Xu X, Yu L, Li R, Peng Q. Benzo[d]thiazole based wide bandgap donor polymers enable 19.54% efficiency organic solar cells along with desirable batch-to-batch reproducibility and general applicability. Adv Mater 2023;35:1–10. https://doi.org/10.1002/adma.202300631.
[15] Peng W, Lin Y, Jeong SY, Genene Z, Magomedov A, Woo HY, et al. Over 18% ternary polymer solar cells enabled by a terpolymer as the third component. Nano Energy 2022;92:106681. https://doi.org/10.1016/j.nanoen.2021.106681.
[16] Jin K, Xiao Z, Ding L. 18.69% PCE from organic solar cells. J Semiconduct 2021;42:18–20. https://doi.org/10.1088/1674-4926/42/6/060502.
[17] Zhu L, Zhang M, Xu J, Li C, Yan J, Zhou G, et al. No Titleהכי קשה לראות את מהשבאמת לנגד העינים. Nat Mater 2022;21:656–63.
[18] Cui Y, Xu Y, Yao H, Bi P, Hong L, Zhang J, et al. Advanced materials - 2021 - cui - single-junction organic photovoltaic cell with 19 Efficiency.pdf. Adv Mater 2021;33:2102420.
[19] Zhou L, Meng L, Zhang J, Zhu C, Qin S, Angunawela I, et al. Adv funct materials - 2021 - zhou - introducing low-cost pyrazine unit into terpolymer enables high-performance Polymer.pdf. Adv Funct Mater 2022;32:2109271.
[20] Yu R, Wu G, Tan Z. Realization of high performance for PM6:Y6 based organic photovoltaic cells. J Energy Chem 2021;61:29–46. https://doi.org/10.1016/j.jechem.2021.01.027.
[21] Guo Q, Guo Q, Geng Y, Tang A, Zhang M, Du M, et al. Recent advances in PM6:Y6-based organic solar cells. Mater Chem Front 2021;5:3257–80. https://doi.org/10.1039/d1qm00060h.
[22] Yuan X, Zhao Y, Zhan T, Oh J, Zhou J, Li J, et al. A donor polymer based on 3-cyanothiophene with superior batch-to-batch reproducibility for high-efficiency organic solar cells. Energy Environ Sci 2021;14:5530–40. https://doi.org/10.1039/d1ee01957k.
[23] Wu J, Fan Q, Xiong M, Wang Q, Chen K, Liu H, et al. Carboxylate substituted pyrazine: a simple and low-cost building block for novel wide bandgap polymer donor enables 15.3% efficiency in organic solar cells. Nano Energy 2021;82:105679. https://doi.org/10.1016/j.nanoen.2020.105679.
[24] Fan Q, Su W, Meng X, Guo X, Li G, Ma W, et al. High-performance non-fullerene polymer solar cells based on fluorine substituted wide bandgap copolymers without extra treatments. Sol RRL 2017;1:1–10. https://doi.org/10.1002/solr.201700020.
[25] Zhang Q, Kelly MA, Bauer N, You W. The curious case of fluorination of conjugated polymers for solar cells. Acc Chem Res 2017;50:2401–9. https://doi.org/10.1021/acs.accounts.7b00326.
[26] Liao Z, Xie Y, Chen L, Tan Y, Huang S, An Y, et al. Adv funct materials - 2019 - liao - fluorobenzotriazole FTAZ -based polymer donor enables organic solar cells exceeding 12.pdf. Adv Funct Mater 2019;29:1808828.
[27] Song CE, Kim YJ, Suranagi SR, Kini GP, Park S, Lee SK, et al. Impact of the crystalline packing structures on charge transport and recombination via alkyl chain tunability of DPP-based small molecules in bulk heterojunction solar cells. ACS Appl Mater Interfaces 2016;8:12940–50. https://doi.org/10.1021/acsami.6b01576.
[28] Kini GP, Hoang QV, Song CE, Lee SK, Shin WS, So WW, et al. Thiophene-benzothiadiazole based D-A1-D-A2 type alternating copolymers for polymer solar cells. Polym Chem 2017;8:3622–31. https://doi.org/10.1039/c7py00696a.
[29] Pang S, Zhang R, Duan C, Zhang S, Gu X, Liu X, et al. Alkyl chain length effects of polymer donors on the morphology and device performance of polymer solar cells with different acceptors. Adv Energy Mater 2019;9:1–12. https://doi.org/10.1002/aenm.201901740.
[30] Zhao F, He D, Xin J, Dai S, Xue H, Jiang L, et al. Modulating morphology via side-chain engineering of fused ring electron acceptors for high performance organic solar cells. Sci China Chem 2019;62:790–6. https://doi.org/10.1007/s11426-019-9453-7.
[31] Yang Y, Liu Z, Zhang G, Zhang X, Zhang D. The effects of side chains on the charge mobilities and functionalities of semiconducting conjugated polymers beyond solubilities. Adv Mater 2019;31:1–32. https://doi.org/10.1002/adma.201903104.
[32] Dang D, Yu D, Wang E. [32]Advanced materials - 2019 - dang - conjugated donor acceptor terpolymers toward high-efficiency polymer solar Cells.pdf. Adv Mater 2019;31:1807019.
[33] Lee J, Lee SM, Chen S, Kumari T, Kang SH, Cho Y, et al. Organic photovoltaics with multiple donor–acceptor pairs. Adv Mater 2019;31:1–17. https://doi.org/10.1002/adma.201804762.
[34] Sun H, Liu T, Yu J, Lau TK, Zhang G, Zhang Y, et al. A monothiophene unit incorporating both fluoro and ester substitution enabling high-performance donor polymers for non-fullerene solar cells with 16.4% efficiency. Energy Environ Sci 2019;12:3328–37. https://doi.org/10.1039/c9ee01890e.
[35] Yang N, Cheng Y, Kim S, Huang B, Liu Z, Deng J, et al. Random copolymerization strategy for host polymer donor PM6 enables improved efficiency both in binary and ternary organic solar cells. ChemSusChem 2022;15:1–8. https://doi.org/10.1002/cssc.202200138.
[36] Chen X, Liao C, Deng M, Xu X, Yu L, Li R, et al. Improving the performance of PM6 donor polymer by random ternary copolymerization of BDD and DTBT segments. Chem Eng J 2023;451:139046. https://doi.org/10.1016/j.cej.2022.139046.
[37] Cui Y, Yao H, Hong L, Zhang T, Xu Y, Xian K, et al. Achieving over 15% efficiency in organic photovoltaic cells via copolymer design. Adv Mater 2019;31:1–7. https://doi.org/10.1002/adma.201808356.
[38] Cheng Y, Jin H, Oh J, Huang X, Lv R, Huang B, et al. Structural similarity induced improvement in the performance of organic solar cells based on novel terpolymer donors. J Mater Chem A 2021;9:9238–47. https://doi.org/10.1039/d1ta00971k.
[39] Wu J, Li G, Fang J, Guo X, Zhu L, Guo B, et al. Random terpolymer based on thiophene-thiazolothiazole unit enabling efficient non-fullerene organic solar cells. Nat Commun 2020;11:1–9. https://doi.org/10.1038/s41467-020-18378-9.
[40] Kim JH, Song CE, Shin N, Kang H, Wood S, Kang IN, et al. High-crystalline medium-band-gap polymers consisting of benzodithiophene and benzotriazole derivatives for organic photovoltaic cells. ACS Appl Mater Interfaces 2013;5:12820–31. https://doi.org/10.1021/am401926h.
[41] Kim JH, Lee M, Yang H, Hwang DH. A high molecular weight triisopropylsilylethynyl (TIPS)-benzodithiophene and diketopyrrolopyrrole-based

copolymer for high performance organic photovoltaic cells. J Mater Chem A 2014; 2:6348–52. https://doi.org/10.1039/c4ta00535j.
[42] Zhu E, Luo G, Liu Y, Yu J, Zhang F, Che G, et al. Triisopropylsilylethynyl substituted benzodithiophene copolymers: synthesis, properties and photovoltaic characterization. J Mater Chem C 2015;3:1595–603. https://doi.org/10.1039/c4tc02107j.
[43] Tamilavan V, Liu Y, Lee J, Jung YK, Son S, Jeong J, et al. Highly crystalline new benzodithiophene-benzothiadiazole copolymer for efficient ternary polymer solar cells with an energy conversion efficiency of over 10. J Mater Chem C 2018;6: 4281–9. https://doi.org/10.1039/c8tc00817e.
[44] Wang L, Liu H, Huai Z, Yang S. Wide band gap and highly conjugated copolymers incorporating 2-(triisopropylsilylethynyl)thiophene-substituted benzodithiophene for efficient non-fullerene organic solar cells. ACS Appl Mater Interfaces 2017;9: 28828–37. https://doi.org/10.1021/acsami.7b09253.
[45] Bin H, Gao L, Zhang ZG, Yang Y, Zhang Y, Zhang C, et al. 11.4% Efficiency non-fullerene polymer solar cells with trialkylsilyl substituted 2D-conjugated polymer as donor. Nat Commun 2016;7:1–11. https://doi.org/10.1038/ncomms13651.
[46] Tang Y, Sun H, Wu Z, Zhang Y, Zhang G, Su M, et al. A new wide bandgap donor polymer for efficient nonfullerene organic solar cells with a large open-circuit voltage. Adv Sci 2019;6:1–10. https://doi.org/10.1002/advs.201901773.
[47] Zhang H, Li S, Xu B, Yao H, Yang B, Hou J. Fullerene-free polymer solar cell based on a polythiophene derivative with an unprecedented energy loss of less than 0.5 eV. J Mater Chem A 2016;4:18043–9. https://doi.org/10.1039/c6ta07672f.
[48] Ji Y, Xu L, Hao X, Gao K. Energy loss in organic solar cells: mechanisms, strategies, and prospects. Sol RRL 2020;4:1–17. https://doi.org/10.1002/solr.202000130.
[49] Wan SS, Xu X, Wang JL, Yuan GZ, Jiang Z, Ge GY, et al. Benzo[1,2-b:4,5- b ′] diselenophene-fused nonfullerene acceptors with alternative aromatic ring-based and monochlorinated end groups: a new synergistic strategy to simultaneously achieve highly efficient organic solar cells with the energy loss of 0.49 eV. J Mater Chem A 2019;7:11802–13. https://doi.org/10.1039/c9ta03177d.
[50] Duan T, Gao J, Xu T, Kan Z, Chen W, Singh R, et al. Simple organic donors based on halogenated oligothiophenes for all small molecule solar cells with efficiency over 11. J Mater Chem A 2020;8:5843–7. https://doi.org/10.1039/d0ta00159g.
[51] Kini GP, Oh S, Abbas Z, Rasool S, Jahandar M, Song CE, et al. Effects on photovoltaic performance of dialkyloxy-benzothiadiazole copolymers by varying the thienoacene donor. ACS Appl Mater Interfaces 2017;9:12617–28. https://doi.org/10.1021/acsami.6b12670.
[52] Liu D, Yang B, Jang B, Xu B, Zhang S, He C, et al. Molecular design of a wide-band-gap conjugated polymer for efficient fullerene-free polymer solar cells. Energy Environ Sci 2017;10:546–51. https://doi.org/10.1039/c6ee03489f.
[53] Kini GP, Park HS, Jeon SJ, Han YW, Moon DK. A 2,5-difluoro benzene-based low cost and efficient polymer donor for non-fullerene solar cells. Sol Energy 2020;207: 720–8. https://doi.org/10.1016/j.solener.2020.06.090.
[54] Chao P, Liu L, Zhou J, Qu J, Mo D, Meng H, et al. Multichloro-Substitution strategy: facing low photon energy loss in nonfullerene solar cells. ACS Appl Energy Mater 2018;1:6549–59. https://doi.org/10.1021/acsaem.8b01447.
[55] Kini GP, Choi JY, Jeon SJ, Suh IS, Moon DK. Effects of incorporated pyrazine on the interchain packing and photovoltaic properties of wide-bandgap D-A polymers for non-fullerene polymer solar cells. Polym Chem 2019;10:4459–68. https://doi.org/10.1039/c9py00674e.
[56] Yang J, Uddin MA, Tang Y, Wang Y, Wang Y, Su H, et al. Quinoxaline-based wide band gap polymers for efficient nonfullerene organic solar cells with large open-circuit voltages. ACS Appl Mater Interfaces 2018;10:23235–46. https://doi.org/10.1021/acsami.8b04432.
[57] Kini GP, Lee SK, Shin WS, Moon SJ, Song CE, Lee JC. Achieving a solar power conversion efficiency exceeding 9% by modifying the structure of a simple, inexpensive and highly scalable polymer. J Mater Chem A 2016;4:18585–97. https://doi.org/10.1039/C6TA08356K.
[58] Li S, Ye L, Zhao W, Yan H, Yang B, Liu D, et al. A wide band gap polymer with a deep highest occupied molecular orbital level enables 14.2% efficiency in polymer solar cells. J Am Chem Soc 2018;140:7159–67. https://doi.org/10.1021/jacs.8b02695.
[59] Wu Y, Yang H, Zou Y, Dong Y, Yuan J, Cui C, et al. A new dialkylthio-substituted naphtho[2,3-: C] thiophene-4,9-dione based polymer donor for high-performance polymer solar cells. Energy Environ Sci 2019;12:675–83. https://doi.org/10.1039/c8ee03608j.